Fracture analysis and reservoir characterization of the granitic basement in HDR Soultz project (France)

Albert Genter, Hervé Traineau, Chrystel Dezayes, Philippe Elsass, B Ledesert, A Meunier, Thierry Villemin

Geotherm. Sci. & Tech., 1995 Volume 4(3) pp. 189–214
Reprints available directly from the publisher
Photocopying permitted by license only

FRACTURE ANALYSIS AND RESERVOIR CHARACTERIZATION OF THE GRANITIC BASEMENT IN THE HDR SOULTZ PROJECT (FRANCE)

A. GENTER[1], H. TRAINEAU[1], Ch. DEZAYES[2], Ph. ELSASS[1], B. LEDESERT[3], A. MEUNIER[3] and Th. VILLEMIN[2]

[1]*BRGM, Direction de la Recherche, Département Géophysique et Imagerie Géologique, Avenue de Conçyr, BP 6009, 45060 Orléans, Cedex 2, France*
[2]*Université de Savoie, Laboratoire de Géodynamique, Campus Scientifique, Savoie Technolac, 73376 Le Bourget du Lac Cedex, France*
[3]*Université de Poitiers, Laboratoire de Pétrologie des Altérations Hydrothermales, 40 avenue du Recteur Pineau, 86022 Poitiers Cedex, France*

(Received August 5, 1994)

Within the framework of the European Hot Rock (HDR) Project, the natural fracture geometry of the deep granitic basement in the Upper Rhine Graben has been studied at Soultz-sous-Forêts (France). The porphyritic granite is characterized by hydrothermally altered and fractured sections. Detailed structural analysis of continuous core samples and borehole wall imagery indicates that fracture zones constitute a complex network of fault segments dominated by N-S trends in accordance with the geometry of the local Soultz horst structure.

Some of these fault segments still carry hydrothermal brines. The attitude of the faults is closely related to the rifting of the graben during the Tertiary. The fractures strike in a direction nearly parallel to the maximum horizontal stress. In this favorable situation, hydraulic injection will tend to reactivate natural fractures at low pressures.

Keywords: Hot Dry Rock, natural fractures, granite, Upper Rhine Graben

1. INTRODUCTION

The geometry and hydraulic properties of pre-existing fracture systems are fundamental in the development of Hot Dry Rock (HDR) geothermal reservoirs. Extensive research has been devoted to this subject on the Soultz site in France, within the framework of the European HDR project (Jung, 1991, 1992; Baria *et al.*, 1992; Beauce *et al.*, 1991, 1992, 1994; Pauwels *et al.*, 1991, 1992, 1993).

The Soultz HDR site is located in the Upper Rhine Graben. The target for the development of an artificial heat exchanger is the granite basement that locally is overlain by 1.4 km of sedimentary cover (Kappelmeyer *et al.*, 1991). Two deep exploratory wells have been drilled: the GPK-1 borehole (3600 m deep) provided a 2 km-long section within the granite basement and the EPS-1 borehole (2230 m deep) provided a 0.8 km-long continuously cored section. The two wells are only 500 m apart. A borehole location plan and a regional structural map are given in Beauce *et al.* (1994) and Benderitter and Elsass (1994).

Geological investigations include borehole monitoring (Genter and Traineau, 1991, 1993), drill core studies (Genter and Traineau, 1992a; Traineau *et al.*, 1991; Ledesert, 1993), well logging data and borehole imagery interpretation (Genter *et al.*, 1989, 1991; Tenzer *et al.*, 1991, 1992; Traineau *et al.*, 1991; Genter and Dezayes, 1993a, b). The basement is composed of porphyritic granite with K-feldspar megacrysts, quartz, plagioclase, biotite and hornblende. Minor petrographic variations, such as K-feldspar clusters and fine-grained xenoliths, have been observed in EPS-1 drill cores. Leucogranitic sections were identified from well log data in the GPK-1 borehole.

In order to provide both a realistic model of the fracture network and geological criteria for present-day permeability in the basement, an exhaustive characterization of natural fractures and faults was conducted on borehole and core data available in the two deep wells. Natural fractures were the only significant structural heterogeneities present before drilling in the granite. The concept of "fractured zone" has been introduced and can be defined as the clustering of fracture sets intersected by a vertical well on a short drilled section. Fractures induced by drilling were also studied from core data and borehole imagery in order to obtain information on the stress field.

2. GEOMETRIC CHARACTERIZATION OF THE NATURAL FRACTURE NETWORK

2.1 EPS-1 Core Analyses

A complete survey of macroscopic natural fractures in granite was carried out from continuous coring in well EPS-1 between 1420 and 2230 m (Genter and Traineau, 1992a). The core sections were oriented by comparison with borehole televiewer imagery (Tenzer *et al.*, 1992). About 3000 natural fractures were identified and classified in order to determine the basic characteristics of the fracture network. Fractures are not homogeneously distributed but are organized in clusters (Ledesert *et al.*, 1993). High density fracture zones are located at the top of the batholith (1420-1530 m), between 1620 and 1655 m, between 2050 and 2080 m and in a permeable brine-producing interval between 2155 and 2180 m (Fig. 1). Other intervals with intermediate fracture density are observed around 1710, 1770, 1810, 1900 and 2220 m. The maximum fracture density is 34 per meter at a depth of about 1650 m. Within this major fracture zone, tectonized facies such as breccia, microbreccia and isotropic or oriented cataclasites are observed. A high concentration of fractures is correlated with hydrothermal alteration (Fig. 1). Natural percolation in fractures induces dissolution of those minerals (plagioclase, biotite) which are the most reactive to hydrothermal alteration. Percolation also results in crystallization of clay minerals (illite) which seal the fractures themselves and their surroundings. The dissolution creates a secondary porosity whereas the crystallization tends to decrease this porosity by the sealing effect.

In EPS-1, natural sealed fractures are organized in two principal fracture sets striking N005°E and N170°E with dips of 70°W and 70°E respectively (Fig. 2A, 2B).These two main sets are close to a conjugate fracture pattern of normal faults related to the formation of the Rhine Graben (Villemin, 1986). The histogram of fracture dips shows that these raw data, i.e. uncorrected for the bias induced by sampling in a vertical borehole, indicate steep dips (Figs. 3A, 4A). Subhorizontal

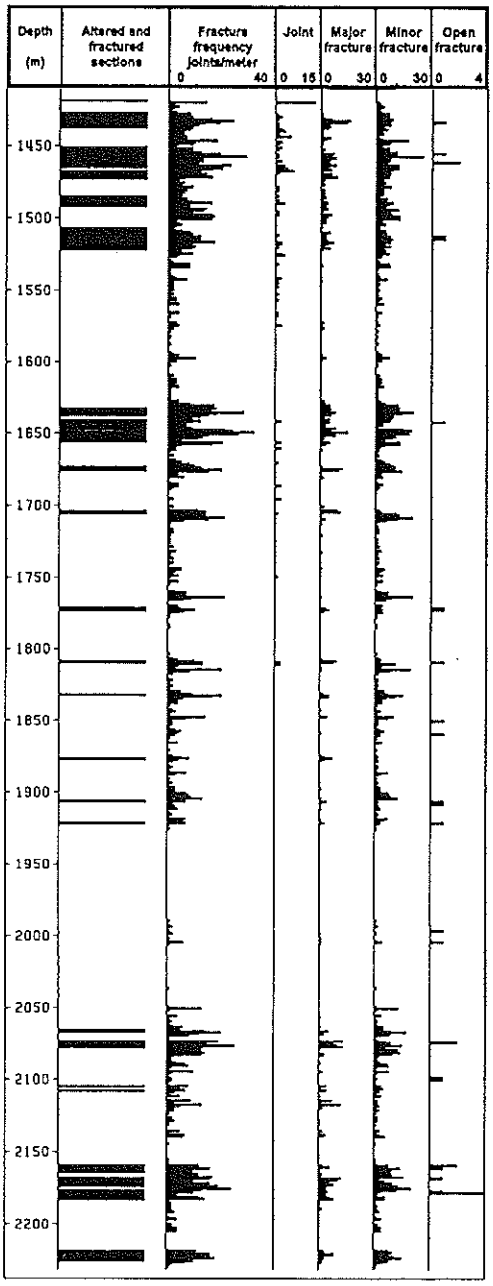

Figure 1 Petrographic log of well EPS-1 showing the location of altered and fractured sections and fracture distribution (overall population, subhorizontal joints, major and minor sealed fractures, open fractures) observed on the core sections from well EPS-1.

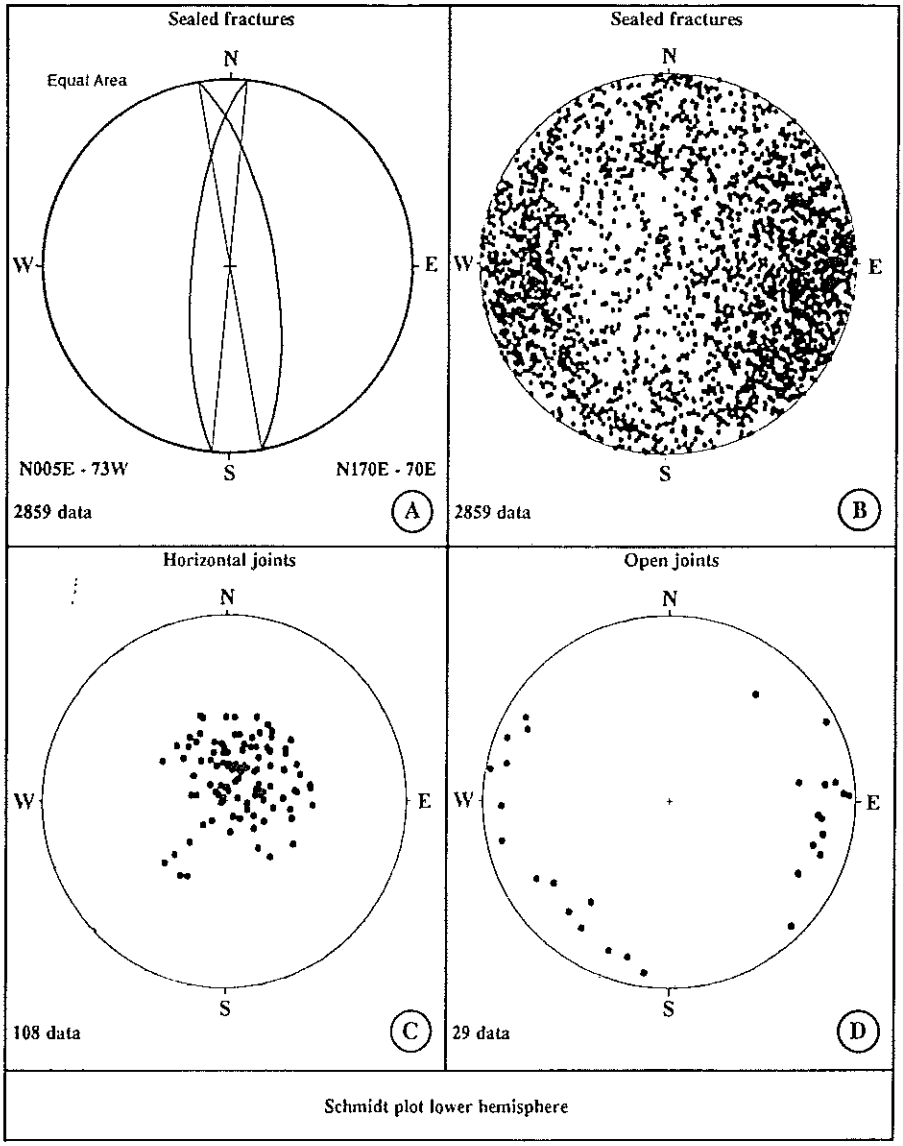

Figure 2 Orientation of the natural sealed fractures observed on EPS-1 core sections. Lower hemisphere projections of the cyclographical construction of principal natural fracture sets (A), of poles to natural sealed fractures (B), of poles to subhorizontal joints (C) and of poles to open fractures (D).

joints do exist but they are present only at the top of the granite basement (Fig. 1). They are interpreted as relaxation joints due to the uplift of the basement (Genter and Traineau, 1992a), and dip at shallow angles to the SSW (Fig. 2C).

Less than thirty natural fractures showing a free aperture or indicators of potential permeability such as geodic veins were observed. Their average free aperture is 1 mm.

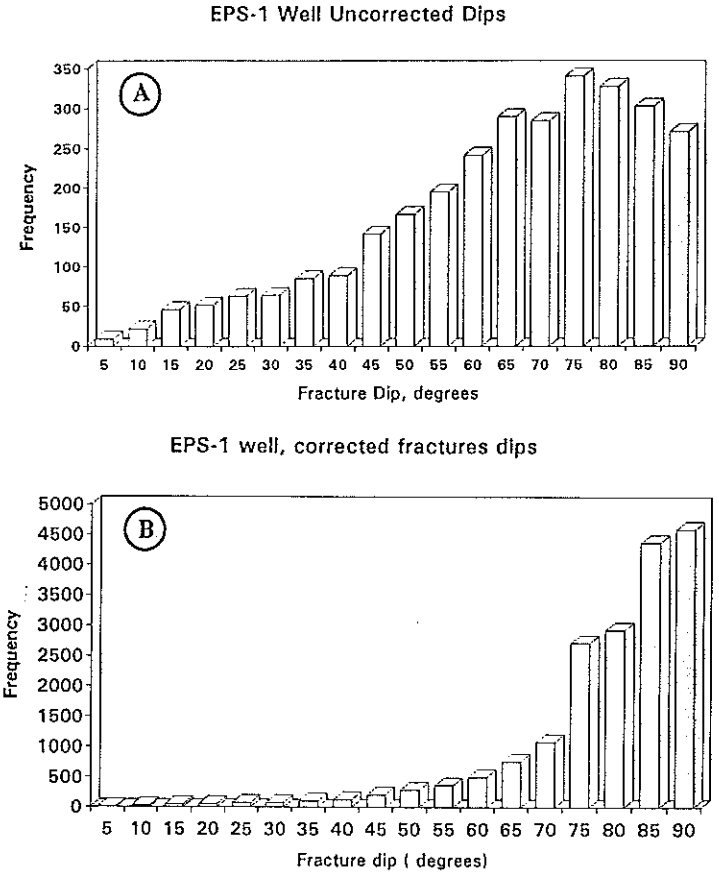

Figure 3 Frequency histograms of fracture dips between 0 and 90° for all the natural fracture populations ($N = 2996$ data) observed on the EPS-1 core sections. (A) Uncorrected dip values. (B) Corrected dip values according to the method of Terzaghi (1965).

The thickest sealed fracture is a 250 mm thick quartz vein at 2175 m depth within an artesian level. The occurrence of geodic quartz seems related to activity of the present-day hydrothermal system (Genter and Traineau, 1992a; 1992b, 1993). Open fractures are mainly located within hydrothermally altered and fractured zones (Figure 1). It is difficult to make a significant statistical interpretation of the attitude of open fractures due to their limited number (29 data, Figure 2D). They appear to belong to a principal fracture set striking N-S (N05E 75W) in the deeper part of the borehole, and a secondary fracture set, at the top of the granite, oriented NW-SE (N130E 65 N).

In order to investigate the bias due to sampling of fractures by a vertical or slightly deviated borehole, a correction factor inverse to the cosine of the angle between fracture plane and drillhole axis, as suggested by R. Terzaghi (1965) and by Barton and Zoback (1992), was applied to the entire set of structural raw data. In a vertical or slightly deviated borehole, the probability of intersecting a horizontal joint is maximal and the corresponding correction therefore negligible. In contrast, for a vertical joint,

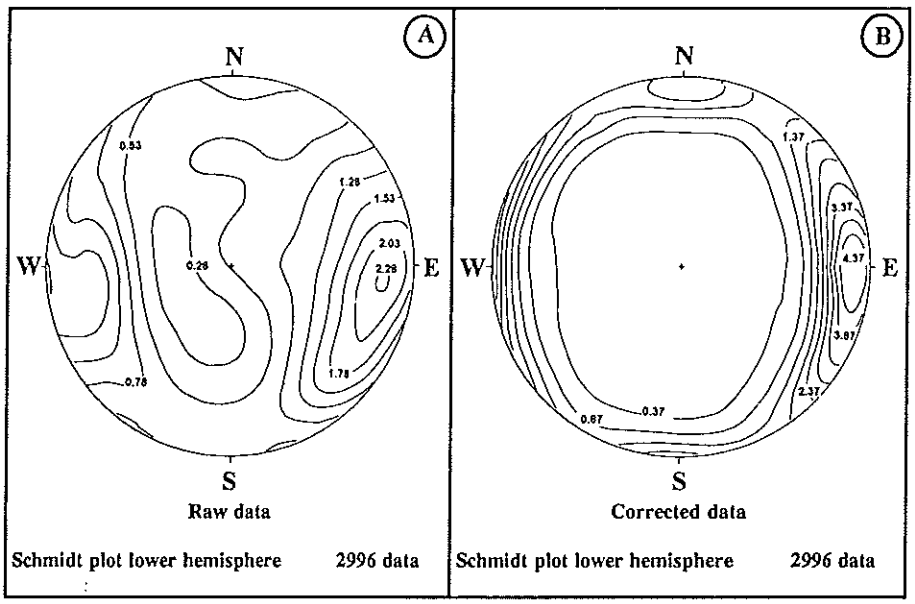

Figure 4 Lower-hemisphere density projections of natural fractures recorded on EPS-1 core sections (A) before and (B) after correction for borehole sampling bias according to the method of Terzaghi (1965).

this probability tends to zero and therefore, the correction should be maximum. A weighting coefficient was computed from the Terzaghi correction for all the fractures recorded on the EPS-1 cores. This weighting factor, used basically for stereographic plotting, emphasizes the role of a vertical fracture set by minimizing the importance of horizontal joints. When the correction is negligible, the weighting coefficient is 1. For the highest correction values, this factor was limited to 100, which may be considered as a very high figure. For the complete set of data, its average value is 6.1 with a standard deviation of 13.0. Figure 5 presents the distribution of this coefficient versus depth. The slight difference between the vertical part (1420–1830 m) and the deviated part (1830–2230 m) of EPS-1 is not very significant; the relative concentration of low values at the top of the basement is related to the abundance of horizontal relaxation joints, and the deviation of the borehole varies between 15 and 20° from vertical at 2100-2200 m depth. All the fractured sections show a similar distribution of this factor which varies continuously between low and high values.

Stereographic projections (Fig. 4A, 4B) comparing raw and corrected data show a general smoothing of the horizontal fracture set and a slight increase of the dip value for steeply dipping fracture sets coupled with an enhancement of the latter. In terms of orientations, an anti-clockwise vertical rotation of 10° can be discerned for the fracture set dipping west.

The distribution of fracture dips after correction appears to follow a positive exponential law (Figure 3B). As expected, this statistical correction increases the number of steeply dipping fractures since 90% of them show a dip value greater than

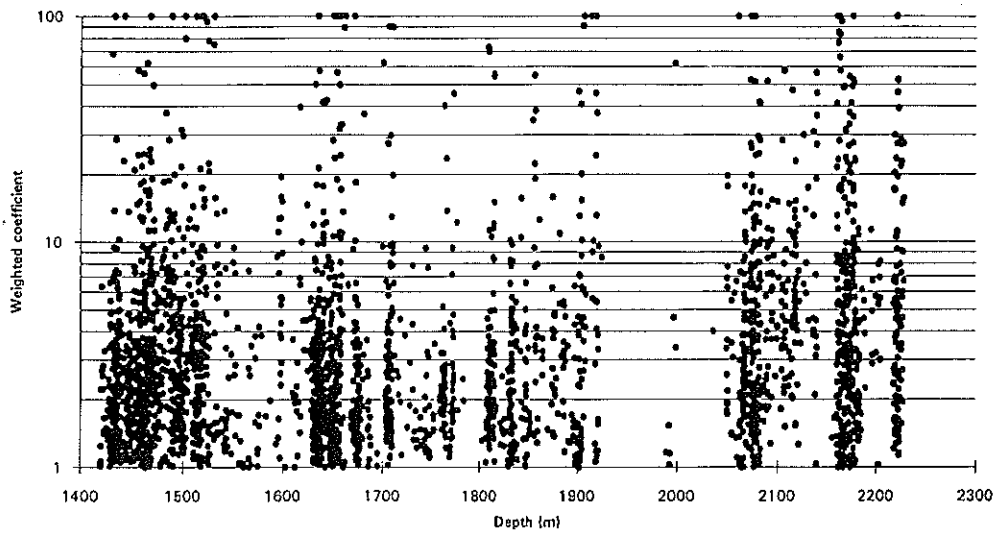

Figure 5 Distribution of calculated weighting factor in a semi-logarithmic plot for all the natural fractures ($N = 2996$ data) observed between 1410 and 2230 m in well EPS-1.

80°, emphasizing the importance of the subvertical fracture network within the Soultz granite.

About 750 major sealed fractures bearing striations and thick filling show a predominant attitude very similar to that of the general fracture system. A selection of the thickest sealed fractures (Fig. 6) shows the principal N-S trending fracture sets (N0E 80 W, N165E 80 E), which are associated with a secondary data set trending NW-SE (N120E 75 N).

A detailed analysis of natural fractures within the major permeable fractured zone (2155-2183 m) shows that the well-defined principal fracture set carrying brine strikes N-S (N0E 80W) but is rather scattered in azimuth (Fig. 7). Two other NE-SW and E-W minor fracture sets are associated to this dominant submeridian fracture set.

About 680 small drilling-induced fractures without any sealing material were observed on EPS-1 cores. They only penetrate a part of the core section plane, and may be present on only one side of the core or on both sides, in which case they form a conjugate fracture system dipping toward the core center. Only 634 of these were reoriented by comparison with borehole imagery. Their distribution with depth seems partly dependent on the pre-existing state of fracturing of the granite. Genter and Traineau (1992) have shown that these induced fractures develop mainly in unaltered granite where natural fracture density is low. Very few induced fractures were observed at the top of the granite, probably because core relaxation was taken up by the numerous natural fractures.

A general clockwise rotation of fracture azimuth is observed with depth (Fig. 8). The strike rotates gradually from NNW-SSE at the top of the granite to NE-SW at the bottom of the hole. When the borehole axis coincides with one of the principal stress directions, the azimuth of drill-induced fractures is thought to be related to the azimuth

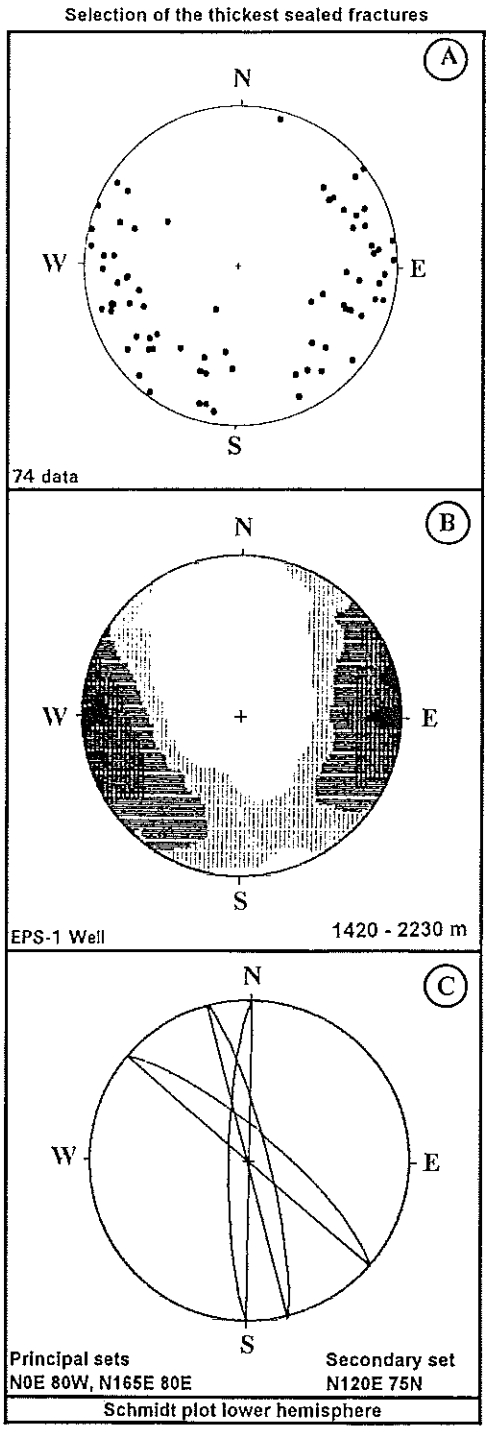

Figure 6 Lower hemisphere projections of poles to a selection of the thickest sealed fractures observed on EPS-1 core sections between 1420 and 2230 m (A), their density equal area projection (B) and cyclographical construction of principal natural fracture sets (C).

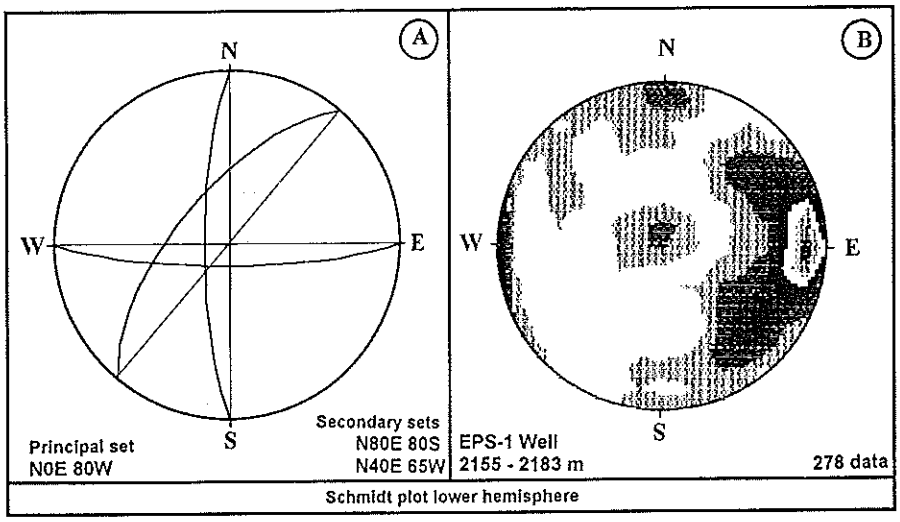

Figure 7 Cyclographical equal area (A) and lower hemisphere density (B) projections of principal natural fracture sets within the master fault zone of EPS-1 well (2155–2183 m) showing permeability.

of the maximum horizontal stress direction (Mastin, 1988). However, this clockwise rotation of core instabilities observed in EPS-1 is probably not related to a rotation of the present stress field but rather to the inclination of the well, which is significantly deviated from vertical below 1830 m.

2.2 FMI Borehole Imagery Interpretation in Well GPK-1

During the deepening of borehole GPK-1 from 2000 to 3600 m, a clear relationship was observed between the drilling rate (Socomine data) and the petrophysical properties of the granite basement (Fig. 9). High drilling rates (> 6 m/h) characterize altered granite zones with fracturing and hydrothermal alteration. In fresh granite, drilling rates fell to around 3 m/h. This was a very useful complement, in locating fractured and altered intervals, to the examination of cuttings (Genter and Traineau, 1993).

The FMI tool provides images of the electrical resistivity of the borehole wall. Resistive points appear as lightcolored spots, conductive parts appear black. An exhaustive fracture evaluation using FMI images (Formation Microscanner Imager, Schlumberger data provided by Socomine) has been performed between 1960 and 3570 m depth in borehole GPK-1 (Genter and Dezayes, 1993a, b). The FMI images were interpreted on site using the FMI Image software (Barton, 1988; modified by Huber, personal communication) installed by Socomine on a Macintosh computer:

a) Typology of planar structures The planar structures intersecting the borehole wall (and imaged as sinusoids) do not all have the same origin. A typology of planar discontinuities was therefore attempted in order to assess the geometry of the pre-existing fracture network and the role of drilling-induced fractures. The structures were classified into natural fractures, segment fractures, en-echelon fractures and vertical induced fractures.

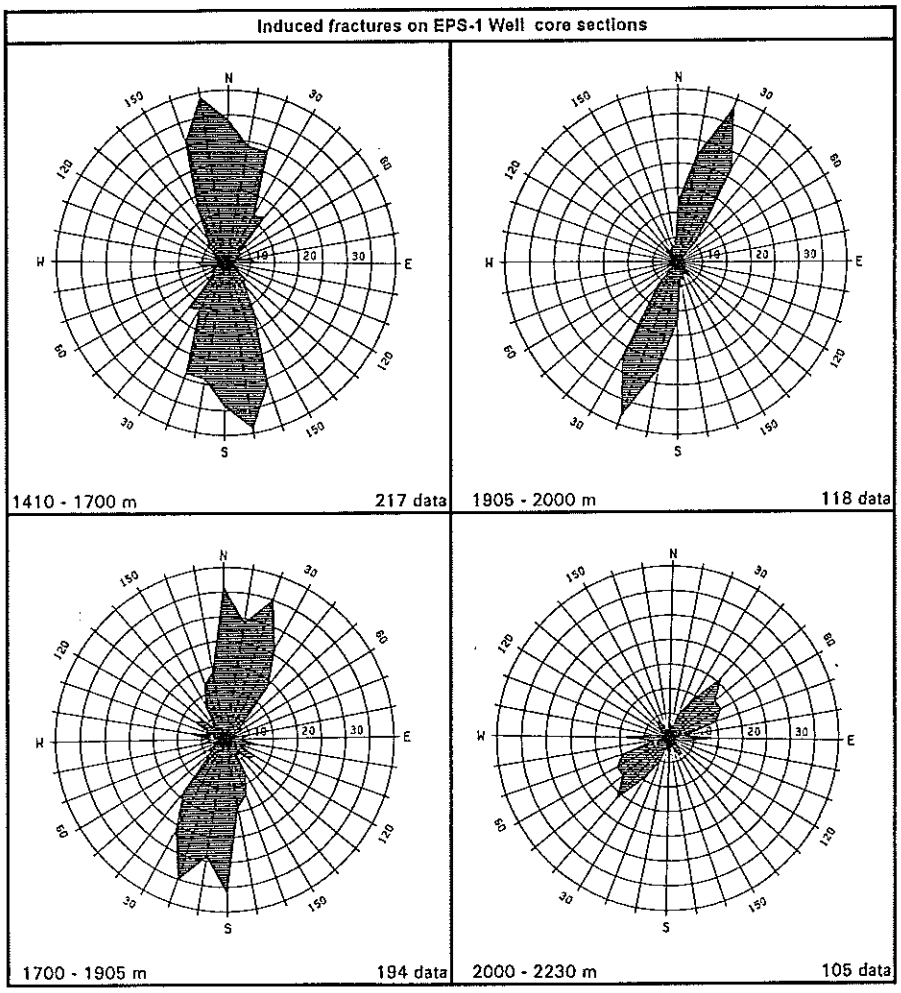

Figure 8 Rose diagrams of strike azimuth for drilling-induced fractures in well EPS-1.

Natural fractures These fractures are the most easily detectable on the borehole image. They are characterized by a continuous dark trace indicating that they are rather conductive. Two main types can be distinguished:

(i) Natural fractures appearing as a dark-colored sinusoidal trace within white resistive surrounding granite (Fig. 10 A, B, C).

(ii) Natural fractures appearing as a dark-colored sinewave trace within a similar dark-colored altered granite. Because of the high conductivity of the granite induced by alteration it is difficult to identify all the fractures in this setting. However, the general attitude of the fractured and altered section can be determined from the orientation of its upper and lower limits (Fig. 10A).

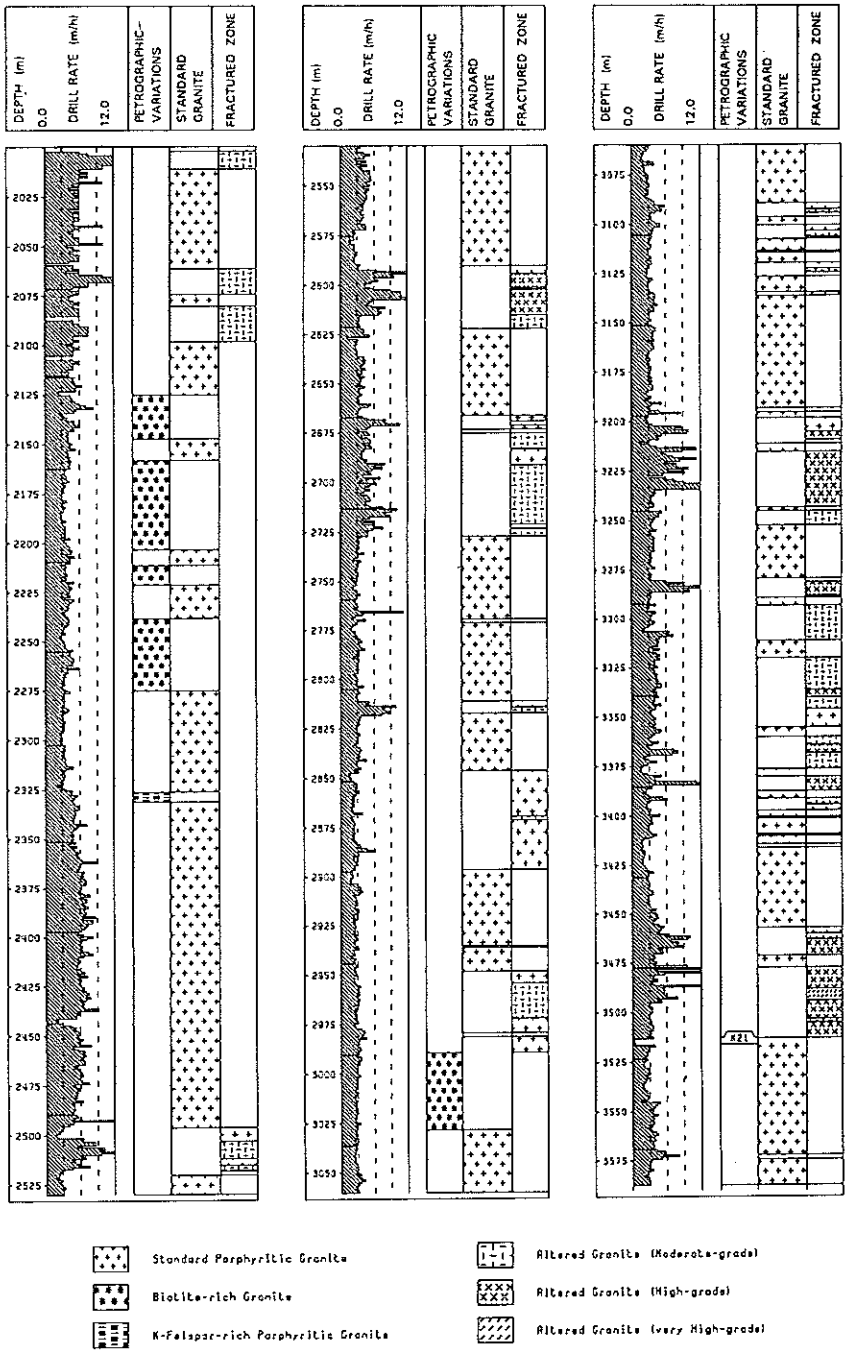

Figure 9 Petrographic log of borehole GPK-1, between 2000 and 3600m, based on chip samples (from Genter and Traineau, 1993). Fractured and altered sections correlated strongly with sharp increase in drill rates.

Figure 10 Examples of borehole imagery responses within the Soultz granitic basement (well GPK–1), Schlumberger data provided by Socomine. A—Two hydrothermally altered and fractured sections appear as dark-colored sinusoidal traces on an oriented FMI image. B—Detection of conductive fractured sections (dark-colored sinusoidal traces) on a Schlumberger Azimuthal Resistivity Imager (ARI) image. C—Detection of natural conductive fractures (dark-colored sinusoidal traces) within light-colored resistive granite on an oriented-FMI image.

Some natural fractures are limited by a rather irregular alteration halo producing a spotted image of the granite, caused by selective alteration of plagioclase and biotite. It was not possible to determine the nature of the hydrothermal products sealing the fractures except for occurrences of white filling which could correspond to quartz veins observed on chip samples during geological monitoring (Genter and Traineau, 1993).

Segment fractures Basically, segment fractures can be described as discontinuous features appearing as half-sinusoidal traces (Fig. 11A). They occur in groups, which may or may not be spatially associated with natural or en-echelon fractures. At least 15 groups of segment fractures have been observed in GPK-1 over different depth intervals. Their shapes, corresponding to the upper and lower parts of a sinusoid, suggest that they have a limited extension beyond the borehole wall. They could be interpreted as drilling-induced fractures.

En echelon fractures These correspond to discontinuous sinusoidal traces showing two symmetrical, steeply dipping limbs (Fig. 11B). These features, which occur within massive granite, are organized in parallel sets. The extremities of the sinusoidal traces are never present. As for segment fractures, the en-echelon fractures have a limited extension. On the borehole images, features transitional between segment and en-echelon fractures are often observed.

Vertical induced fractures These structures are characterized by a subvertical dip and cut the borehole wall over several meters length (Fig. 11C). They are well developed through massive granite and are associated with steeply dipping natural fractures. Their extension into the granite also seems rather limited and they are interpreted as fractures induced by stress and/or thermal shock during drilling.

b) Classification of fractures according to apparent electrical width The varying electrical contrast between the borehole wall and the fracture results in the image varying in width and darkness. An apparent electrical width was recorded for each

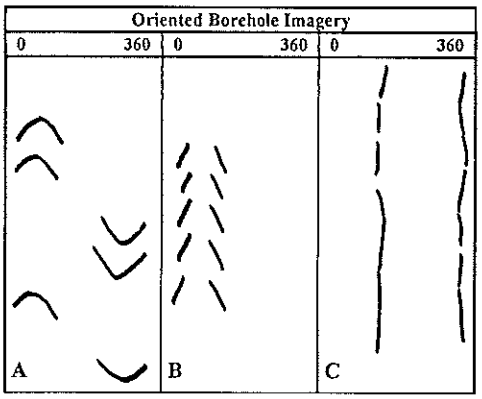

Figure 11 Schematic views of segment fractures (A), en-echelon fractures (B) and vertical induced fractures (C) on borehole wall imagery.

interpreted feature, and the fractures are grouped into three categories: narrow (n. 787), average (n. 184) and wide (n. 23) fractures. These sizes are not directly proportional to the true width or the aperture of fractures but are related to their ability to conduct electrical current.

c) Fracture frequency Between 1960 and 3570 m, 994 fractures were recorded from FMI image interpretation, including 589 natural fractures, 180 segment fractures, 208 en-echelon fractures and 17 vertical drilling-induced fractures. The vertical discontinuities have not been systematically measured. Table I gives the fracture frequency per meter in GPK-1 obtained from borehole images. These results are compared with those obtained from continuous coring in well EPS-1 and from borehole imagery or spot coring in the upper part of GPK-1 well.

The natural fracture density per meter measured from BHTV images in well EPS-1 (0.64) is much lower than the densities observed on EPS-1 core sections (3.7). For the upper part of well GPK-1, BHTV fracture density is rather similar to core fracture density (3.24 as against 3.80) but BHTV data mixed natural and induced fractures probably inducing an overestimation of the resulting fracture density. The natural fracture density measured from FMI images in well GPK-1 (0.54 to 0.72) shows the same order of range as BHTV results in EPS-1 (0.64). For the electrical images, these results could be explained by the combination of two different factors:

(i) In hydrothermally altered and fractured intervals, the images are dark and electrically noisy due to alteration, so that many fractures are not detectable.
(ii) The present stress field is likely to have reactivated most of the fracture planes that are subparallel to the major horizontal stress direction. These fractures would be slightly open and conductive because they are impregnated by saline drilling fluid, and would be imaged preferentially. In contrast, pre-existing fractures subperpendicular to the major horizontal stress direction are likely to be less reactivated and therefore would not be well imaged.

Table I
Fracture frequency from FMI images in two different sections of GPK-1, compared with previous results obtained by different methods in the upper parts of wells GPK-1 and EPS-1

Borehole	Depth interval (m)	Method	References	Frequency joints/meter	Type
GPK-1	1960–2870	FMI 8 pads	Genter, Dezayes, 1993b	0.54	natural
GPK-1	2870–3570	FMI 8 pads	Genter, Dezayes, 1993a	0.72	natural
GPK-1	1420–2000	FMS 4 pads	Genter, 1989 Genter *et al.*, 1991	0.96	natural
GPK-1	1420–2000	BHTV	Tenzer *et al.*, 1991	3.24	natural and induced
GPK-1	1420–2000	spot coring (43 m length)	Genter, 1989 Genter *et al.*, 1991	3.80	natural
EPS-1	1420–2230	BHTV	Tenzer *et al.*, 1991	0.64 0.60	natural induced
EPS-1	1420–2230	continuous core sections	Genter, Traineau, 1992	3.70 0.74	natural induced

Comparison of the density of drilling-induced fractures is not reliable because they were not systematically recorded and they do not have the same behavior on core sections as on the borehole surface.

d) Orientation of the fracture network from FMI data Stereographic projections of the complete population of fractures observed on FMI (994 data) indicate three principal fracture sets striking N010E, N020E and N175E and dipping 65E, 70W and 65W respectively (Fig. 12 A, B); west-dipping fracture sets are dominant. Two secondary fracture sets striking NW-SE to NNW-SSE (N145E 70W, N160E 60E) can also be distinguished. Schmidt diagrams for natural fractures, segment fractures and en-echelon fractures (Fig. 12 C, D, E) show two major fracture sets for all origins, striking N-S and dipping steeply west or east. The two secondary sets are present in the diagram for natural fractures. The stereographic projection of vertical induced fractures indicates only one principal set striking N-S (Figure 12 F).

Twenty three fractures were classified as having a large apparent electrical width. These should correspond to principal potential permeable pathways within the granitic basement (Fig. 13). They strike N-S or NNE-SSW (N170E 65W, N025 70E and 70W). A secondary fracture set has a NW-SE trend (N130E 70N).

2.3 Fracture Attitude in the Sedimentary Cover

The interpretation of BHTV (Borehole Televiewer, Stadtwerke Bad Urach data) ultrasonic imaging from a neighbouring borehole (seismic detection borehole 4550), gives the attitude of fractures within Lower Triassic sandstones (Buntsandstein) which directly overlie the Soultz granite. A major, probably hydraulically active, permeable fault zone was intersected during drilling at about 1260 m depth; it strikes N170E with a dip of 75W.

Natural fractures in Buntsandstein core sections recovered from well EPS-1 show a pure conjugate relationship, striking N170E and dipping 75W and E. In this fully cored well, there is no evidence of present day permeability in these sedimentary levels.

3. GEOMETRIC CHARACTERISATION OF THE HYDROTHERMALLY ALTERED AND FRACTURED ZONES

3.1 The Concept of a Hydrothermally Altered and Fractured Zone

Natural fractures are organized in clusters within the granite. High fracture density promoted fluid circulation which resulted in significant hydrothermal alteration characterized by the deposition of clay minerals. A high concentration of single fractures grouped in different directional fracture sets and related vein alteration together define a hydrothermally altered volume of rock.

Examination of the EPS-1 cores (Genter and Traineau, 1992) revealed a general spatial pattern. Fracture zones are organized with a core of intense fracturing in which breccia, microbreccia and oriented cataclasites developed, corresponding to successive stages of brittle deformation. The primary minerals of the granite have been dissolved, and the fractures have commonly been sealed by geodic quartz veins several centimeters thick. Surrounding the core is an intermediate zone in which fracturing is less

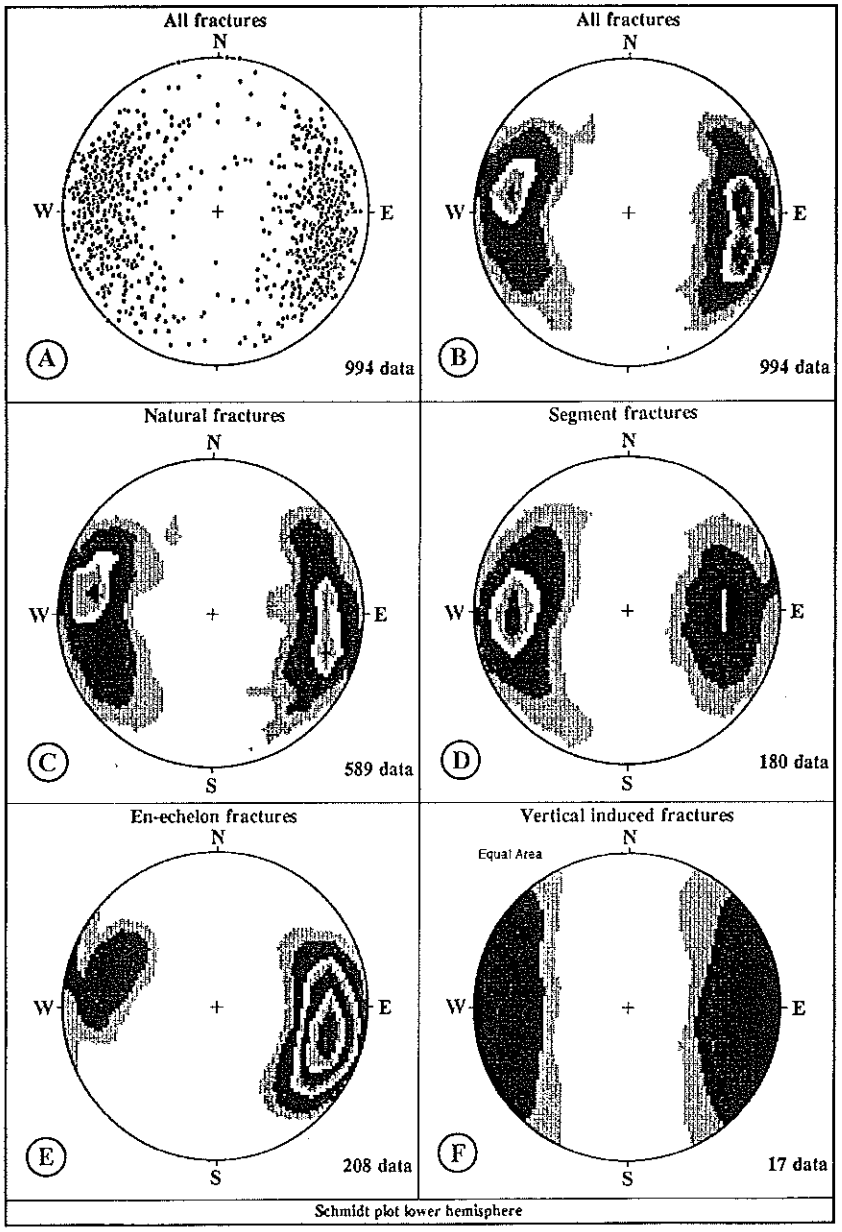

Figure 12 Orientation of natural fractures from FMI borehole imagery in well GPK-1 between 2000 and 3600 m. Lower hemisphere projections of poles to all the fractures (A) and their density plot (B); density plots of natural fractures (C), segment fractures (D), en-echelon fractures (E) and induced fractures (F).

intense. Cataclastic granite is present in this zone and hydrothermal alteration is less intense than in the central part. Lastly, an outer zone is characterized by low fracture density but fairly intense alteration of plagioclase and biotite, which are readily transformed into clay minerals. This outer zone is considered as altered wall rock.

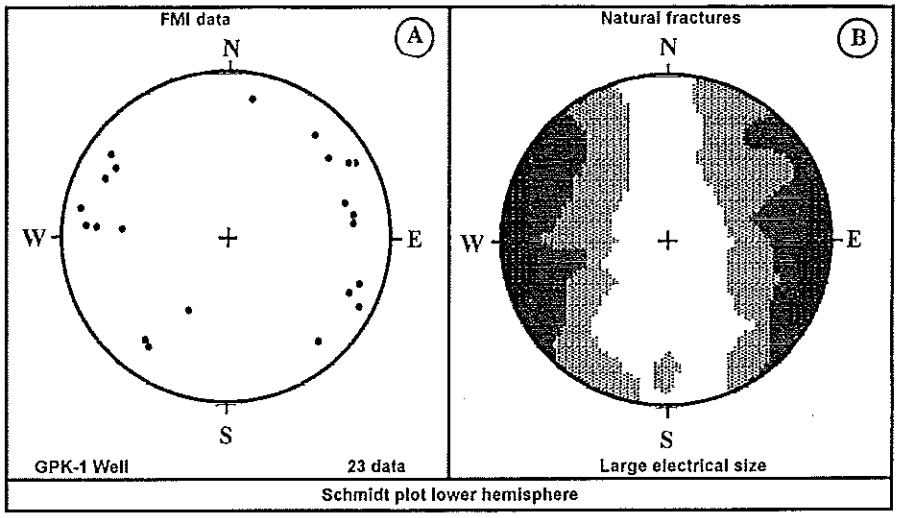

Figure 13 Orientation of 23 selected natural fractures with large apparent electrical width observed on an oriented FMI borehole image in well GPK-1 between 2000 and 3600 m depth. Lower hemisphere projections of their poles (A) and density plot (B).

Because of their ability to detect petrophysical variations between massive and altered granitic rock, conventional wireline logs (neutron porosity, sonic velocity, nuclear density) were used in combination with geological logging of the two deep wells to locate accurately the upper and lower limits of each altered zone, and thus determine an apparent vertical width.

The geometric characteristics of an isolated joint plane can be measured on core samples or from oriented borehole imagery. The evaluation of the same characteristics for an altered zone is much more difficult owing to the high concentration of fractures. Assuming that they probably play a major role as fluid pathways within the fractured basement, it is of prime importance to determine the attitude of each zone. Moreover, we consider that they have their own geometric characteristics (dip direction, dip, apparent vertical length) which are not necessarily similar to those of each discrete fracture set.

Thirty-nine fractured intervals and twelve fractured intervals respectively were investigated in GPK-1 and EPS-1. For each interval, a mean orientation and a mean dip were evaluated from a variety of types of oriented borehole imagery (BHTV, FMI, FMS-4 pads, ARI from Socomine/Schlumberger and DMT data). Only in the most favorable cases could both hanging wall and footwall of a given zone be measured with confidence. A quality ranking was therefore established to take into account the uncertainty in measurement. The upper and lower limits of a given interval are not systematically parallel, and an assumption was necessary for the selection of the most appropriate limit. For instance, clear open fractures or perfect continuous sinusoids visible on borehole imagery were assumed to characterize best the attitude of a complete interval.

3.2 Geometry of Hydrothermally Altered and Fractured Zones

a) Width of fractured zones Each fractured zone corresponds to a drilled section in which fractures are clustered; a given zone therefore shows an apparent vertical length. Knowing the average dip of a fractured zone and its apparent vertical length, a true width can be computed. The average true width is about 3 m, with a minimum of 0.2 m and a maximum of 28.5 m. The histogram of the width of fractured zones, expressed by metric class, appears to follow approximately a log-normal law (Fig. 14). This is consistent with the findings of studies on simple fractures (Loiseau, 1987).

b) Attitudes of fractured zones In wells GPK-1 and EPS-1 the distribution of the attitudes of fractured and altered zones, although widely scattered (Fig. 15), shows a maximum of orientations striking N-S and dipping 65 W. In GPK-1, there is no significant trend in variation of the attitudes of fractured zones with depth. Between 1420 and 2000 m, the N160E + 15° azimuth is dominant and between 2000 and 3600 m, the orientation is N180E + 10°. Two secondary sets striking N140E + 10° and N020E + 10° and both dipping west can also be distinguished. In contrast, a change in strike azimuth of fractured and altered zones with depth can be clearly seen in well EPS-1. Fracture zones between 1420 and 1700 m strike N140E + 15° and those at greater depths (1700–2220 m) strike N180E + 20°, like those GPK-1. Some dip values are subhorizontal. The deepest concentration of fractured and altered zones is at 2170 m depth, striking N015E, and is composed of several potentially permeable subzones dipping west.

The attitudes of fractured sections measured with good reliability were grouped into high quality ranking zones. They have a mean N-S (N175E) strike with a subvertical dip. This corresponds to the average attitude of induced fractures, which is thought to represent the plane of the major hozirontal and vertical directions of the present-day

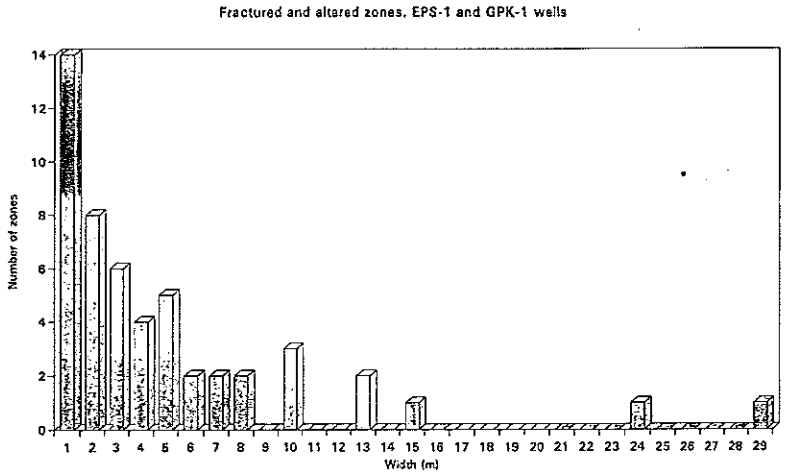

Figure 14 Frequency histogram of the width of fractured and hydrothermally altered sections encountered in wells EPS-1 and GPK-1 (N = 51).

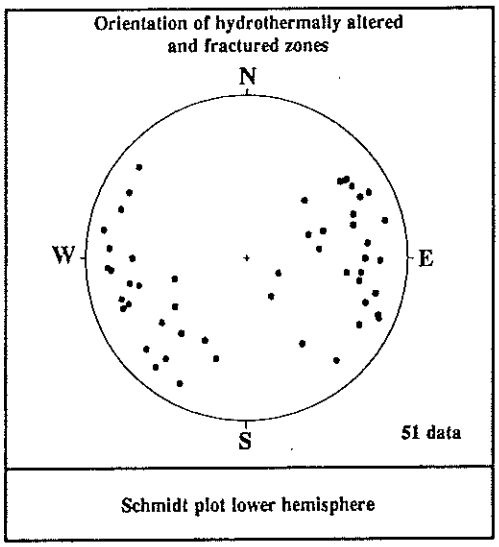

Figure 15 Lower hemisphere projection of poles to hydrothermally altered and fractured sections encountered in wells EPS-1 and GPK-1.

stress field. The stereographic projection of the poles of the hydrothermally altered and fractured zones (Fig. 15) shows a distribution very close to the distribution of open fractures recorded on cores (Fig. 2D).

c) Cross-sections intersecting EPS-1 and GPK-1 Schematic vertical cross-sections, through EPS-1 and GPK-1 oriented N90E (Figure 16) show that the fractured zones are not randomly distributed along the vertical. They are concentrated in two intervals in well EPS-1 and three intervals in well GPK-1. These concentrations can be interpreted as the trace of megascopic faults in the granite basement, with individual fractured and altered sections representing segments of these faults. The average vertical distance between two successive megascopic faults ranges between 300 m and 400 m. In well GPK-1, the average spacing between two successive individual hydrothermally altered and fractured zones is about 50 m.

The three concentrations of fractured and altered zones encountered in GPK-1 at 1800, 2750 and 3400 m depth, show common features:

(i) two conjugate sets, one of them prominent,
(ii) the presence of at least one permeable section within each concentration of fractured zones,
(iii) orientations consistent with the Oligocene Rhine rifting with strikes of N160E to N180E.

Except for the N140E set in the upper part of well EPS-1, the attitude of fractured and altered zones is consistent with orientation of the E-W extensional regime of Tertiary times.

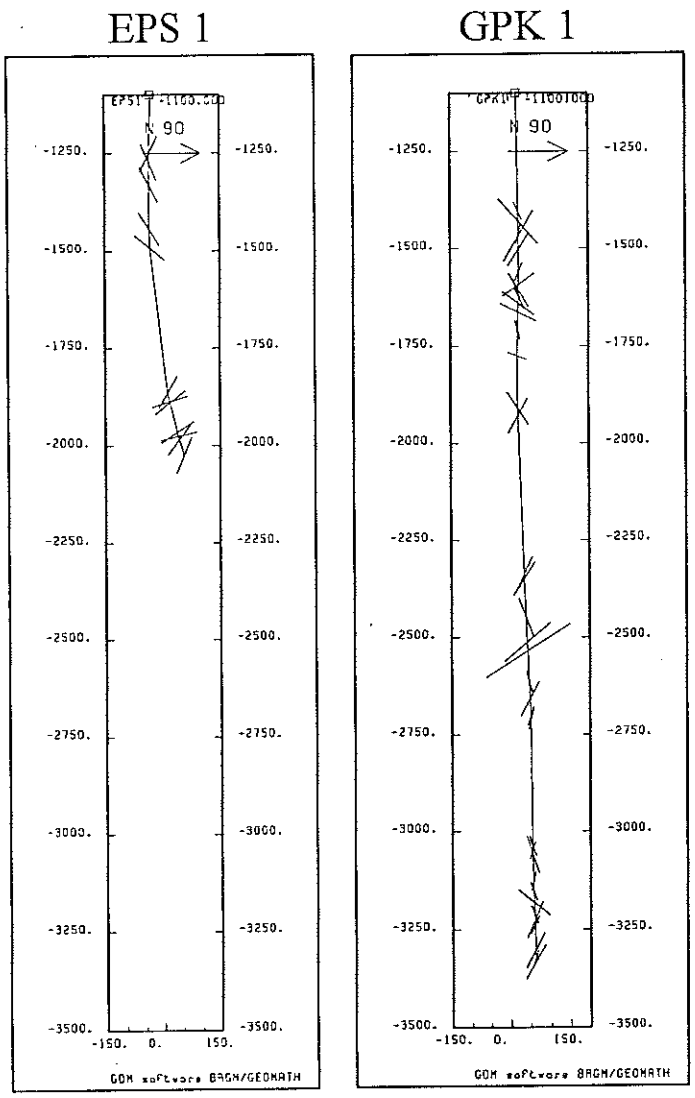

Figure 16 Cross-sections oriented N090E in well EPS-1 and well GPK-1 showing the locations of the hydrothermally altered and fractured sections. The length of the bars is proportional to the true width of the sections. Depths are expressed in meters above the sea level. Lateral deviation from the borehole collar locations is also expressed in meters.

4. PRESENT-DAY PERMEABILITY INDICATORS

Pauwels *et al.* (1993), on the basis of the chemical composition of deep geothermal saline fluids sampled in the Upper Rhine Graben, concluded that the waters encountered in the deep sedimentary fractured reservoirs and in the fractured granitic basement had a common origin. Two fractured and altered sections in well GPK-1

(1816 m, 3493 m) and one in well EPS-1 (2150-2180 m) produced hot salt brines (100 g/l) during drilling. This present-day permeability seems to be closely related to open fractures partly sealed by late geodic quartz deposits and characterized by extensive wall-rock illitization. Detailed petrographic studies have revealed the presence of tosudite (a regular dioctahedral chlorite and smectite mixed-layer lithium-bearing mineral) and of organic compounds within the producing zone in well EPS-1 (Ledesert, 1993). The organic matter has probably been transported through the fracture network from overlying or deep sedimentary reservoirs (Fig. 17). This indicates that hydrothermal convection cells may develop along or perpendicular to major normal faults affecting both the sedimentary rocks and the granitic basement (Flores Marques, 1992). As the normal faults at Soultz strike mainly N-S and dip west, this suggests that fluid recharge may take place on the west flank of the Rhine Graben.

However, Pauwels *et al.* (1993), propose a hypothesis, based on geochemical and geothermometric data, in which the origin of the fluids is deep on the eastern flank, in contradiction with our geometric considerations. The question of the pathways (eastern or western) for present-day circulation therefore remains unresolved.

Anomalies in gases such as methane, helium, radon and carbon dioxide were also recorded during the drilling-mud survey when well GPK–1 penetrated fractured and altered granitic sections (Vuataz *et al.*, 1990; Aquilina *et.al.*, 1993). These anomalies generally coincided with a sharp increase in drilling rate. These permeability indicators probably reflect the lower cohesion of the rock in response to fracturing and its soft

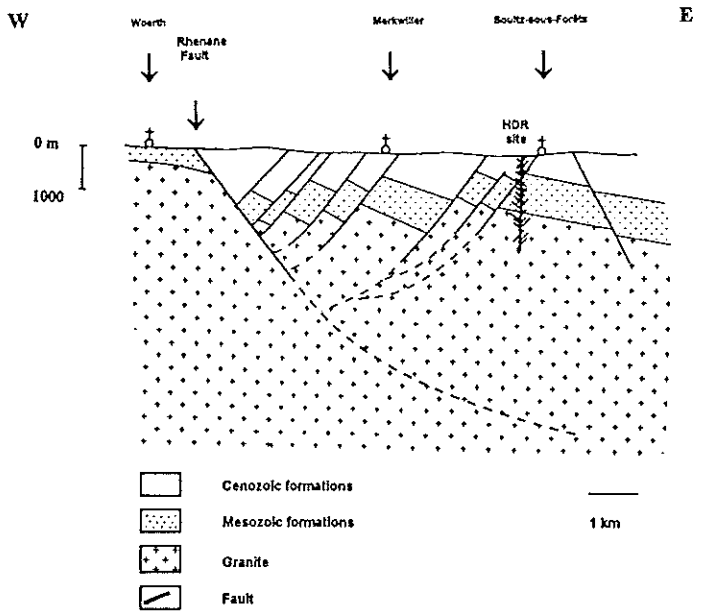

Figure 17 Schematic E-W cross-section of the Upper Rhine Graben in the Soultz area. (From Brun *et al.*, 1992; modified by Dezayes, 1992). Mesozoic formations include the deep Triassic sandstones which constitute an aquifer.

nature caused by the extensive development of clay minerals. Permeable fractured zones detected during drilling (Genter and Traineau, 1992a, b, 1993; Aquilina *et al.*, 1993) are oriented according to two principal directional sets (Table II), N-S to NNE-SSW and NW-SE to ESE-WNW and dip west or north.

5 DISCUSSION AND CONCLUDING REMARKS

Fracturing in the Soultz granite was surveyed in detail on core and borehole imagery and analysed to provide a realistic geometric model of the fracture network. The results are limited in space to the scale of the two deep wells, GPK–1 and EPS–1.

5.1 Geometry of Hydrothermally Altered and Fractured Zones Related to Rifting

Detailed analysis of fault populations in the Rhine Graben area (Villemin, 1986; Bergerat, 1987) has distinguished four main stages of brittle tectonics during the Tertiary (Table III). Dezayes (1992) showed from EPS-1 core analysis that at least three extensional tectonic stages occurred during the Mesozoic but their precise nature was

Table II
Characteristics of the permeable hydrothermally altered and fractured sections in wells GPK-1 and EPS-1

Well	Depth (m)	Orientation	True Thickness (m)	Permeability indicators
GPK-1	1820	N117E 47N	7.20	Gas, brines, quartz, illite
GPK-1	2815	N142E 68W	2.50	Gas, illite
GPK-1	3385	N020E 68W	3.00	Gas, illite
GPK-1	3492	N007E 61W	4.30	Gas, brines, quartz, illite
EPS-1	2170	N015E 37W average value	22.50	Brines, quartz, illite

Table III
Cenozoic paleostress fields and associated brittle structures affecting the Upper Rhine graben and its surrounding area (Villemin, 1986, Villemin and Bergerat, 1987)

Age	Stress field	Orientation of main brittle structures
Late Miocene to Present	NW-SE compression	N-S sinistral shears WNW-ESE dextral shears
Miocene	NE-SW compression	N-S dextral shears E-W to ESE-WNW sinistral shears
Oligocene	E-W extension	N-S to NNE-SSW normal faults
Eocene	N-S compression	NW-SE dextral faults NE-SW NNE-SSW to N-S sinistral faults

difficult to determine owing to a lack of striated fault planes. Some of the major rift faults were formed as sinistral strike-slip faults during the N-S Eocene compressive stage (Villemin and Bergerat, 1987). During the Oligocene, the subsidence of the graben took place in an E-W extensional regime. This major extensional event was responsible for the formation of a local horst-like structure at Soultz (Fig. 17).

Single natural fractures are clustered in zones affected by a wide halo of hydrothermal alteration, creating a reservoir-like volume. These zones can be interpreted as segments of megascopic faults. The orientations of the fracture zones, except for the transverse directions in the upper part of EPS-1 are consistent with the Oligocene extensional regime; the faults were thus generated or reactivated during the opening of the Rhine Graben. They divide the granitic basement into N-S blocks several hundred meters wide. However, the scatter of fracture distribution suggests that a transverse fault inherited from older tectonic phases (NW-SE, NE-SW, ESE-WNW) probably exists, complicating the geometry of the basement.

In well GPK-1, the three major faults have similar geometries, so that guidelines can be proposed for their modelling. Each fault contains two subconjugate, steeply dipping sets of fracture zones striking N-S, one set being numerically predominant. If a correlation is assumed between lateral extension and width, the main set probably has the greater extension. In addition, active drains have been detected in each of the faults.

In well EPS-1, these basic guidelines cannot be applied as there is only one directional data set for a given fault zone, and its orientation is not typically that of the Rhine rifting (Fig. 15). The lack of any eastward-dipping fracture zone in the deeper part of EPS-1 could be explained by the trajectory of the well, which deviates at depth by 15° to 20° eastward from the vertical and becomes subparallel to the dip of the non-intersected faults. Moreover, the absence of eastward-dipping fault zones in well EPS–1 could be explained by the proximity of the Western Rhine fault. This is a major normal synthetic fault which compensates the sets of antithetic normal faults (Fig. 17) forming the western part of the Soultz horst structure (Dezayes, 1992; Dezayes *et al.*, 1993).

5.2 Geometry of the Pre-existing Fracture System

Continuous coring data (well EPS-1) show that the orientation of natural fractures is fairly constant with depth except at the top of the basement. They are characterized by a N-S strike and both easterly and westerly dips. Fracture orientations are less systematic within major fracture zones, however; for example in well EPS-1 between 2155 and 2183 m, a permeable major fault zone comprises three subzones, the lowest and the highest of which trend N-S whereas the intermediate zone shows a principal fracture set with an E-W strike (Fig. 7).

The main fracture sets oriented N170E are almost conjugate (Fig. 2A). Since its emplacement, the Soultz granite has undergone several successive episodes of brittle deformation which have greatly influenced the geometry of the existing fracture system. Its situation within the Rhine graben has meant that the Rhine fault direction is over-represented relative to earlier-formed fractures. The main fracture sets at Soultz are therefore probably the result of the reactivation of former fractures by the major

tectonic events which have affected the area, the N-S Eocene compressive and the E-W Oligocene extensional episodes.

5.3 Geometry of the Fracture System and Permeability

A permeable fracture network exists within the Soultz granite. In the deeper parts of both EPS-1 (2150–2180 m) and GPK-1 (2180 m, 3390 m, 3493 m), the hydraulically active fractured zones dip to the west. A similar result was found at 1260 m depth in the Triassic sandstones of well 4550 (drilled during the same project), 500 m away, which intersects a major fault striking N170E with a dip of 75W.

The presence of illite and geodic quartz are not discriminant indicators of present day permeability as they have been observed within both active and fossile hydrothermally altered zones. The occurrence of tosudite or organic matter within the main EPS-1 permeable zone seems to be another good indicator of large scale vertical fluid circulation between the oil-bearing sedimentary beds and the granitic basement (Ledesert, 1993).

Resistivity borehole imagery shows that the main fracture sets strike N-S even in the deeper part of well GPK-1. Comparison with core data shows that not all the fractures are systematically sampled by electrical multipad tools. Within hydrothermally altered and fractured zones, the presence of clay minerals and the high porosity result in high conductivity, obscuring the image of a number of fractures (Figure 10A). Whatever the origin of segment or en-echelon fractures, their occurrence is related to the maximum horizontal stress direction. These fractures are either reactivated pre-existing planes or have been induced by stress and thermal shock. The FMI tool seems thus preferentially to image fractures which are slightly open, i.e. subparallel to S_H max because they are filled with saline drilling mud. In-situ hydraulic tests in borehole GPK-1 have indicated that the maximum horizontal stress is oriented N148E, stress magnitude measurements indicating a normal faulting regime (Rummel and Baumgartner, 1991); televiewer data indicate a slightly different orientation, at N170E (Tenzer *et al.*, 1991). The pre-existing natural fractures are subparallel to the maximum horizontal stress.

This colinearity is favorable to improving the HDR reservoir performance by re-opening the fractures. The present-day stress field tends to reactivate zones of weakness such as altered fracture zones and consequently to enhance clustering of fractures. This is a favorable situation as hydraulic injection will tend to reactivate natural fractures at lower pressures than those required for hydraulic fracturing.

Acknowledgements

This research has been carried out within the framework of the European hot Dry Rock Project funded by the Commission of the European Communities (DG XII). Geological investigations were supported in part by the scientific research program of BRGM (project EG 22) and in part by the Agence de l'Environnement et de la Maîtrise de l'Energie (Ademe). The authors are grateful to the coordinating organization Socomine which has provided samples, borehole data and helpful assistance on site. Constructive criticism by Andre' Gérard has improved this paper considerably. The manuscript greatly benefitted from the constructive comments of two anonymous reviewers. The English of the final version of the manuscript was improved by John Kemp, BRGM Translation Service.

References

Aquilina, L., M. Brach, JC. Foucher and A. De Las Heras (1993). WELCOM (Well Chemical Online Monitoring): Geochemical logging of Soultz-sous-Forêts granite. Hot Dry Rock geothermal project (Alsace, France). in Proceedings of *European Union of Geosciencess*, EUG VII, Strasbourg, France, 4–8 April 1993, Terra abstracts, Blackwell Scientific Publications, Vol. 5, 452.

Baria, R., J. Baumgärnter, A. Gérard, and O. Kappelmeyer (1992). HDR project at Soultz-sous-Forêts, *Geothermal Resources Council Transactions*, 16, 387–394.

Barton C A. (1988). In-situ stress measurements techniques for deep drillholes, Ph. D. thesis, Stanford, Calif.

Barton, C. A., M. D. Zoback (1992). Self-Similar distribution and properties of macroscopic fractures at depth in crystalline rock in the Cajon Pass Scientific Drill Hole. *Journal of Geophysical Research*, 97(B4), 5181–5200.

Beauce, A., H. Fabriol, D. Le Masne, C. Cavoit, P. Mechler and X. Chen (1991). Seismic studies on the HDR site of Soultz-sous-Forêts (Alsace, France) *Geotherm. Sci. Tech.*, 3(1–4), 239–266.

Beauce, A., R. Jones, H. Fabriol, C. Twose and C. Hulot (1992). Microseismic monitoring of hydraulic experiments undertaken during phase IIa of the Soultz HDR project (Alsace, France), *Proceedings, 17th Workshop on Geothermal Reservoir Engineering*, Stanford University, Stanford, California, January 29–31, SGP-TR-141, 253–258.

Beauce, A., R. Jones, H. Fabriol, and C. Hulot (in press). Seismic studies on the Soultz HDR Project (France) during phase IIa: (accepted for publication in *Geotherm. Sci. and Tech.*).

Benderitter, Y., and Ph. Elsass (in press). Deep fluid circulations at the Soultz HDR site (accepted for publication in *Geotherm. Sci & Tech.*).

Bergerat, F., (1987). Paléo-champs de contraintes tertiaires dans la plate-forme européenne au front de l'orogéne alpin, *Bull. Soc. Geol. Fr., III*, 3, 611–620.

Brun J. P., M .A. Gutscher and Dekorp-Ecors teams (1992). Deep crustal structure of the Rhine Graben from Dekorp-Ecors seismic reflection data: a summary, *Tectonophysics*, 208, 139–147.

Dezayes, Ch. (1992). Etude de la fracturation dans les forages géothermiques de Soultz-sous-Forêts. *Rapport de stage de DEA*, Université de Savoie (Chambéry)., 103 p.

Dezayes, Ch.,Th. Villemin, A. Genter, H. Traineau and J. Angelier (1993). Paleostress analysis from fault and fracture geometry in the Hot Dry Rock boreholes at Soultz-sous-Forêts (Rhine graben), in proceedings of *European Union of Geosciences*, EUG VII, Strasbourg, France, 4–8 April 1993, Terra abstracts, Blackwell Scientific Publications, Vol. 5, 217.

Flores Marques E. L. (1992). Transferts de chaleur et de masse en milieu sédimentaire et fracturé. Modélisation numérique de la convection naturelle autour du site géothermique de Soultz. Thése de Doctorat de l' Institut National Polytechnique de Lorraine, 18 juin 1992, 229 p.

Genter, A. (1989). Géothermie Roches Chaudes Séches: le granite de Soultz-sous-Forêts (Bas-Rhin, France). Fracturation naturelle, altérations hydrothermales et interaction eau-roche. Ph.D. thesis, 201 p. Univ. of Orleans, Orleans.

Genter, A., J. P. Cautru, P. Montaggioni and H. Traineau (1989). Geological interpretation of well logging data from the granitic section of the Soultz-sous-Forêts GPK–1 well. SPWLA, in proceedings of *12th International Well Logging Symposium*, SAID, paper EE, 25–27 Oct. 89, Paris, 12 p.

Genter, A. and H. Traineau (1991). The European HDR project (Soultz, France): preliminary geological results from the deep borehole EPS-1. European Union of Geosciences EUG VI 24–28 March 91, Strasbourg, Terra Nova, vol. 3, number 1, 448–449.

Genter, A. and Ch. Dezayes (1993a). Fracture evaluation in GPK-1 borehole using FMI data (Soultz-sous-Forêts). *Technical note* RCS 93 T90, Field report, 25-03. 1993, 3 p.

Genter, A. and Ch. Dezayes (1993 b). Fracture evalution in GPK-1 borehole using FMI data between 2870 and 1960 m (Soultz-sous-Forêts). *Technical note RCS 93 T91, Field report*, 24.06, 1993, 5 p.

Genter, A., P. Martin and Ph. Montaggioni (1991). Application of FMS and BHTV tools for evaluation of natural fractures in the Soultz geothermal borehole GPK-1. *Geotherm. Sci. Tech.*, 3 (1–4), 69–82.

Genter, A. and H. Traineau (1992 a). Borehole EPS-1, Alsace, France: Preliminary geological results from granite core analyses for Hot Dry Rock Research. *Scientific Drilling*, 3, 205–214.

Genter. A. and H. Traineau (1992 b). Hydrothermally altered and fractured granite as an HDR reservoir in the EPS-1 borehole, Alsace France. Proceedings, *17th Workshop on Geothermal Reservoir Engineering*, Stanford University, Stanford, California, January 29–31, 1992, SGP-TR–141, 33–38.

Genter, A. and H. Traineau (1993). Deepening of GPK-1 HDR borehole, 2000–3600 m (Soultz-sous-Forêts, France): geological monitoring. *BRGM Open File report SGN R* 36611, 25 p.

Jung, R. (1991).Hydraulic fracturing and hydraulic testing in the granitic section of borehole GPK-1, Soultz-sous-Forêts. *Geotherm. Sci. Tech.*, 3, 149–198.

Jung, R. (1992). Connecting a borehole to a nearby fault by means of hydraulic fracturing. Geothermal Resources Council Transactions, 16, 433–437.

Kappelmeyer, O., A. Gérard. W. Schloemer, R. Ferrandes, F. Rummel and Y. Benderitter (1991).European HDR project at Soultz-sous-Forêts general presentation, *Geotherm. sci. Tech.*, 2(4). 263–289.

Ledesert, B. (1993). Fracturation et paléocirculations hydrothermales. Application aur granite de Soultz-sous-Forêts. *Ph. D. Thesis*, 203 p., Univ. of Poitiers, Poitiers.

Ledesert, B., J. Dubois, A. Genter and A. Meunier (1993). Fractal analysis of fracture applied to Soultz-sous-Forêts. Hot Dry Rock geothermal program. *J. Volcanol. Geotherm. Res.*, **57**, 1–17.

Loiseau, P. (1987). Etude structurale et géostatistique des gneiss de la région du Cézallier. Modélisation tridimensionnelle de réseaux de fractures, application á l'écoulement des fluides, *Ph. D. Thesis*, 182 p, Univ. of Orléans, Orléans.

Mastin, L. (1988). Effect of borehole deviation on breakout orientations, *J.Geophys. Res.* **93**(B8), 9187–9195.

Pauwels, H., A. Criaud, F. D. Vuataz, M. Brach and C. Fouillac (1991). Uses of chemical tracers in HDR reservoirs studies. *Geotherm. Sci. Tech.*, **3**, 83–103.

Pauwels, H., C. Fouillac and A. Criaud (1992). Water-rock interactions during experiments within the geothermal HDR Borehole GPK-1 at Soultz-sous-Forêts (alsace, France). *Applied Geochem.*, **7**, 243–255.

Pauwels, H., C. Fouillac and A. M. Fouillac (1993). Chemistry and isotopes of deep geothermal saline fluids in the upper Rhine Graben: origin of compounds and water-rock interactions. *Geochim. Cosmochim. Acta.*, **57**, 2737–2749.

Rummel, F. and J. Baumgärtner (1991). Hydraulic fracturation measurements in the GPK-1 borehole, Soultz-sous-Forêts. *Geotherm. Sci. Tech.*, **3**(1–4), 119–148.

Tenzer, H., L. Mastin and B. Heinemann (1991). Determination of planar discontinuities and borehole geometry in the crystalline rock of borehole GPK-1 at Soultz-sous-Forêts. *Geotherm. Sci. Tech.*, **3**(1–4), 31–67.

Tenzer, H., P. Budeus and R. Schellschmidt (1992). Fracture analyses in Hot dry Rock drillholes at Soultz and Urach by borehole televiewer measurements. *Geothermal Resources Council Transactions*, **16**, 317–321.

Terzaghi R. (1965). Sources of error in joint surveys. *Geotechnique*, **15**, 287–304.

Traineau, H., A. Genter, JP. Cautru, H. Fabriol and Ph. Chevremont (1991). Petrography of the granite massif from drill cutting analysis and well log interpretation in the HDR borehole GPK-1 (Soultz, Alsace, France). *Geotherm. Sci. Techn.*, **3**(1–4), 1–29.

Villemin, Th. (1986). Tectonique en extension, fracturation et subsidence: le fossé rhénan et le bassin de Sarre-Nahe, Ph. D. Thesis, 270 p., Univ. Pierre et Marie Curie, Paris.

Villemin, Th. and F. Bergerat (1987). L'évolution structurale du Fossé Rhénan au cours du cénozoïque: un bilan de la déformation et des effects thermiques de l'extension, *Bull. Soc. Géol. France (8), t. III*, n° 2, 245–255.

Vuataz, F. D., M. Brach, A. Criaud and C. Fouillac (1990). Geochemical monitoring of drilling fluids: a powerful tool to forecast and detect formation waters. *SPE Formation Evaluation, June*, 177–184.